UCRL-JC-134513
PREPRINT

Thermal Electric and Magnetic Fields at the Surface of an Electron Beam Target

Manuel Garcia

This paper was prepared for submittal to the
26th IEEE International Conference on Plasma Science
Monterey, CA
June 20-24, 1999

June 9, 1999

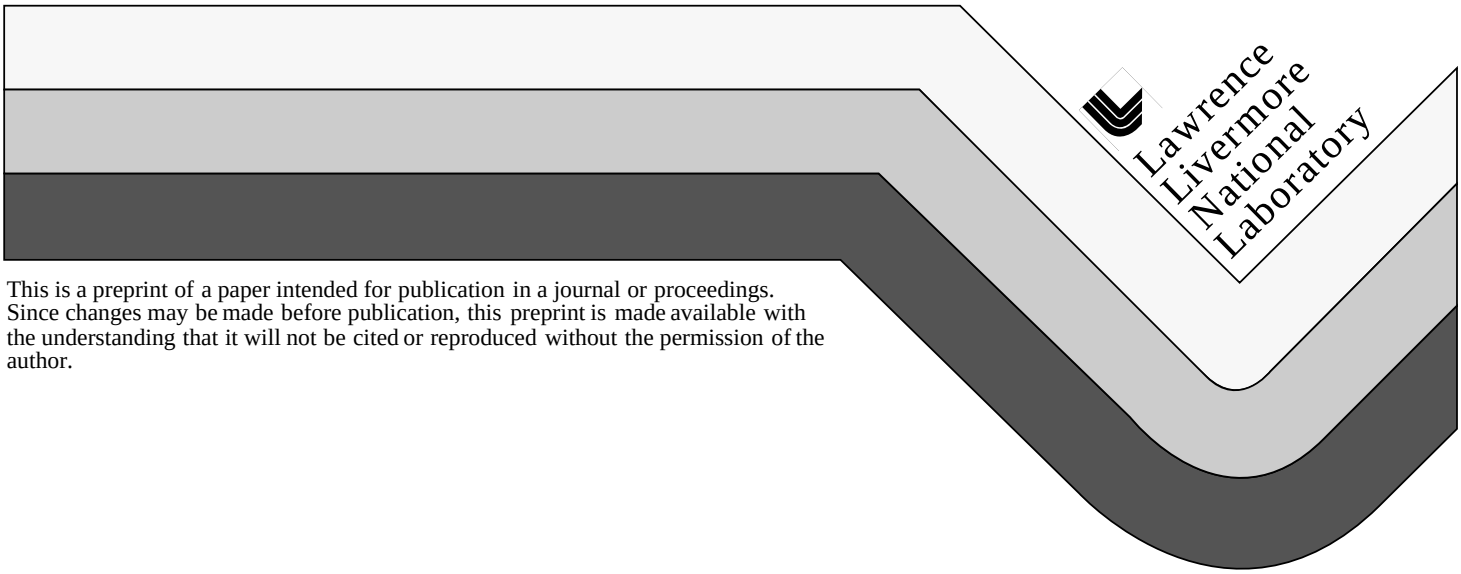

Thermal electric and magnetic fields at the surface of an electron beam target

Manuel Garcia

9 June 1999

Lawrence Livermore National Laboratory, L-153, POB 808 Livermore, CA 94551-0808 USA
garcia22@llnl.gov, (925) 422-6017, FAX (925) 423-5080

A relativistic electron beam pulse of high current density will heat a thin target plate to a plasma state as it traverses. The gradient of plasma temperature ∇T_e is predominantly radial, and the gradient of plasma density ∇n_e is predominantly axial. The cross product of these terms is significant at the vacuum-to-metal interface through which the beam enters. This cross product is a thermal source of magnetization, which can be much larger than the vacuum magnetic field of the electron beam, and it is of opposite polarity. The thermal energy density in the target can be hundreds of times larger than the energy density of the vacuum magnetic field of the beam. If the nose of the electron beam current pulse rises linearly with time then the thermal magnetization increases as time squared. Heat pushes electrons axially from the interior of the plate to the surfaces, and radially away from the beam axis. The electric field that arises from this effect is essentially the negative of the pressure gradient, it points outward.

A continuing work

This report continues the presentation of reference [1] without further introduction. My intent is to make this a brief report, in essence an appendix to reference [1]. Equation numbering will continue the sequence of reference [1], the first new equation in this report is number (70).

This report describes the electric and magnetic fields at the surface of a target during beam entry. My goal is a quixotic one, to prove a negative, which is that bare ions do not emerge from the target plasma to accelerate along the axis of the approaching electron beam. The assumption that such ion flow exists has motivated a great deal of work. These efforts include

space-charge PIC computations predicting the effect [2] and [3], experiments [4], [5], and [6], analysis [7], and computations of remediation schemes [8] and [9]. None of these efforts considers a magnetized target, nor the influence of thermal energy density in producing magnetization. The thermal energy density in the target can be hundreds of times larger than the energy density of the vacuum magnetic field of the beam. How electron beam target magnetization can arise from thermodynamics is described in [1], where the analysis was guided by the extensive work on thermal magnetization in laser-fusion, see [10] and [11].

Electric field at the surface

Inserting the generalized Ohm's law

$$\mathbf{j} = \sigma(\mathbf{E} + \mathbf{v} \times \mathbf{B} + \frac{\nabla p_e}{e n_e}), \tag{36}$$

and the electron beam current density source $\mathbf{j}_0$,

$$\mathbf{j}_0 = \text{curl}(\frac{\mathbf{B}_0}{\mu}), \tag{37}$$

into Ampere's law,

$$\text{curl}(\frac{\mathbf{B}}{\mu}) = \mathbf{j} + \mathbf{j}_0 + \varepsilon\frac{\partial \mathbf{E}}{\partial t}, \tag{38}$$

produces an equation for the electric field,

$$\mathbf{E} = \frac{1}{\sigma\mu}\text{curl}(\mathbf{B} - \mathbf{B}_0) - \mathbf{v} \times \mathbf{B} - \frac{k T_e}{e}(\frac{\nabla T_e}{T_e} + \frac{\nabla n_e}{n_e}), \tag{70}$$

where $p_e = k n_e T_e$. The electric field arises from magnetic diffusion and convection, and from the electron pressure gradient. **B** is itself created thermally.

Consider an idealized model of the vacuum-to-metal interface. Assume this boundary layer has a thickness λ_0. Let r be a radial coordinate parallel to the surface, $x = r/r_0$ for beam radius r_0, and z is an axial coordinate

through the layer, which points into the external vacuum. The functional dependencies are:

$$\mathbf{B} = B_\theta(r, z, t)\mathbf{i}_\theta,$$

$$\mathbf{B}_0 = B_{0\theta}(r, t)\mathbf{i}_\theta,$$

$$\mathbf{v} = v_z(r, z, t)\mathbf{i}_z,$$

$$T_e(r, t) \text{ and } n_e(z, t). \tag{71}$$

Applying (71) to (70) produces component equations:

$$E_r = \frac{-1}{\sigma\mu}\frac{\partial B_\theta}{\partial z} + v_z B_\theta - \frac{kT_e}{e}\left(\frac{1}{T_e}\frac{\partial T_e}{\partial r}\right), \tag{72}$$

$$E_z = \frac{1}{\sigma\mu r}\frac{\partial}{\partial r}\left[r(B_\theta - B_{0\theta})\right] - \frac{kT_e}{e}\left(\frac{1}{n_e}\frac{\partial n_e}{\partial z}\right). \tag{73}$$

Radial and axial derivatives

Radial derivatives are a consequence of the radial profile of the electron beam, and axial derivatives are a consequence of the diminution of density across the layer. The derivatives and factors needed are:

$$\frac{1}{B_\theta}\frac{\partial B_\theta}{\partial z} = \left(\frac{1}{n_e}\frac{\partial n_e}{\partial z}\right), \tag{62}$$

$$\frac{1}{n_e}\frac{\partial n_e}{\partial z} = \frac{-1}{\lambda_0}, \tag{74}$$

$$\frac{1}{T_e}\frac{\partial T_e}{\partial r} = -\left(\frac{12}{r_0}\right)\frac{x}{(1 + 2x^2)}, \tag{49}$$

$$f_J(x) = \frac{1}{(1 + 2x^2)^3}, \tag{46}$$

$$f_B(x) = \frac{x}{(1 + 2x^2)^4}, \tag{60}$$

$$B_{.816}(t) \equiv B_{0\theta}(0.816 r_0, t) = \mu j_0(0, t) r_0/8, \tag{75}$$

$$\frac{\partial B_{0\theta}}{\partial r} = \frac{B_{.816}}{r_0}\left(8 f_J(x) - \frac{B_{0\theta}}{x B_{.816}}\right), \tag{50}$$

$$\frac{r}{B_\theta}\frac{\partial B_\theta}{\partial r} = \frac{1 - 14x^2}{1 + 2x^2}. \tag{61}$$

Equation (74) is a simple model of the boundary layer density profile, equation (75) is a convenient definition, and the other terms were described in [1].

Applying these results to (72) and (73) produces:

$$E_r = \left(v_z + \frac{1}{\sigma\mu\lambda_0}\right) B_\theta + 12\frac{kT_e}{e r_0}\frac{f_B(x)}{f_J(x)}, \tag{76}$$

$$E_z = \frac{kT_e}{e\lambda_0} + \frac{1}{\sigma\mu r_0}\left(\frac{2 - 12x^2}{1 + 2x^2}\frac{B_\theta}{x} - 8 B_{.816}(t) f_J(x)\right). \tag{77}$$

Next, we find B_θ for an electron beam current pulse that rises linearly with time.

B_θ for a linear beam

For a linear beam:

$$j_0(0, t) = j_\infty \frac{t}{t_\infty},$$

$$B_{0\theta}(0.816 r_0, t) = \frac{\mu j_\infty r_0}{8}\frac{t}{t_\infty} = B_\infty \frac{t}{t_\infty},$$

$$\frac{kT_e(0, t)}{e} = \frac{\gamma - 1}{\gamma}\frac{m}{e}\Delta E \frac{|j_\infty| t_\infty}{2}\left(\frac{t}{t_\infty}\right)^2 = \frac{kT_\infty}{e}\left(\frac{t}{t_\infty}\right)^2, \tag{67}$$

where the subscript ∞ indicates quantities at the end of the beam time ramp, and $\Delta E = 1.6 \times 10^5$ (eV/m)/(kg/m^3), which is an average energy loss by collisions as a relativistic electron beam penetrates a target of atomic mass m.

The Faraday law model of equations (65) and (66) results in:

$$K_1 = \frac{-B_\infty}{t_\infty} \frac{f_K(x)}{\sigma\mu r_0^2},$$

$$K_2 = \frac{-kT_\infty}{e} \frac{1}{t_\infty^2} \frac{12}{r_0\lambda_0} f_B(x),$$

$$\omega = \left(v_z - \frac{1}{\sigma\mu\lambda_0} \right) \frac{1}{\lambda_0} - \frac{\partial v_z}{\partial z} + \frac{f_\omega(x)}{\sigma\mu r_0^2}, \qquad (78)$$

which are analogous to source coefficients K_1 and K_2, and relaxation rate ω in (68). The functions f_K and f_ω were defined for equation (63) and are:

$$f_K(x) = \frac{96x}{\left(1 + 2x^2\right)^4} + \frac{1}{x^2}\left[1 - \frac{1}{\left(1 + 2x^2\right)^2}\right],$$

$$f_\omega(x) = \frac{12}{1 + 2x^2} + \left(1 + \frac{18x^2}{1 + 2x^2}\right) \frac{1}{x^2} \left(\frac{1 - 14x^2}{1 + 2x^2}\right) - 16 \frac{3 + 14x^2}{1 + 2x^2}. \qquad (79)$$

The function f_K is positive (x is always positive), while f_ω is negative for $x > 0.152$. The magnetic induction is

$$B_\theta = \frac{K_1}{\omega^2}\left(e^{\omega t} - 1 - \omega t\right) + \frac{K_2}{\omega^3}\left(2e^{\omega t} - 1 - (1 + \omega t)^2\right). \qquad (66)$$

Consider the relaxation rate ω from (78). Assume that v_z is uniform over the short extent in z of the layer. If the boundary layer is static, $v_z = 0$, then the magnetic field leaks away by axial and radial diffusion. If the axial velocity equals the axial magnetic diffusion speed, $v_z = 1/(\sigma\mu\lambda_0)$, then only radial diffusion acts to limit the retention of B_θ. In this case the

magnetic Reynolds number of the boundary layer is unity, $R_M = \sigma\mu v_z\lambda_0 = 1$. If the axial velocity exceeds the axial magnetic diffusion speed then B_θ grows very rapidly. Thus, the expansion of the plasma into the electron beam helps to retain the thermally generated magnetization. This magnetization works to diverge the electron beam, and to bind electron and ion motion to the boundary layer. To estimate the boundary layer motion, use the local thermal speed,

$$v_z = \sqrt{\gamma \frac{kT_e(r, t)}{m}} = \sqrt{\gamma \frac{kT_\infty}{m}\left(\frac{t}{t_\infty}\right)^2 f_J(x)}\ . \qquad (80)$$

Two examples

Figure 1 shows $B_\theta(x, t)$ for a linear beam with $I_0(0, t_\infty) = 6000$ A, $r_0 = 0.5$ mm, $j_\infty = 3.06 \times 10^{10}$ A/m, $t_\infty = 20$ ns, $B_\infty = 2.4$ T, and $kT_\infty/e = 37$ eV, which pierces a boundary layer of tantalum with $\lambda_0 = 2 \times 10^{-5}$ m and $\sigma = 10^6$ S/m. Five radial profiles are shown, at 4 ns, 8 ns, 12 ns, 16 ns, and 20 ns. Negative $B_\theta(x, t)$ values are plotted (positive numbers). $B_{0\theta}$ of the electron beam is positive as electrons move toward negative z. Flux builds up near $x = 0.3$ where the cross product of temperature and density gradients has its peak, and near the axis where radial diffusion is inward and the axial motion is most pronounced. The magnitude of B_θ reaches over –3 T.

Figure 2 shows $E_r(x, t)$ for the example of Figure 1. This radial field points inward below $x = 0.4$, and outward with much lower intensity above this point.

Figure 3 shows the axial electric field $E_z(x, t)$ for the example of Figure 1. This field reaches 1 MV/m by the end of the current ramp, and it points outward.

Figure 4 shows the axial velocity given by (80) for the example of Figure 1. The velocity is such that $R_M < 0.2$.

Figure 5 shows the inverted relaxation rate for the example of Figure 1. This is a local relaxation time. This time is about 0.5 ns over most of the radial profile, but it grows rapidly near the axis.

Figure 6 shows $B_\theta(x, t)$ for a boundary layer with $\lambda_0 = 5 \times 10^{-5}$ m and all other parameters identical to those of the example of Figure 1. Negative

$B_\theta(x, t)$ values are plotted (positive numbers). The magnitude of B_θ reaches over –11 T. The velocity is such that $R_M < 0.5$. B_θ builds up to a higher level because it takes longer to leak out of a thicker layer.

Figure 7 shows $E_r(x, t)$ for the thicker layer, compare this with Figure 2.

Figure 8 shows the axial electric field $E_z(x, t)$ for the thicker layer, compare this with Figure 3.

Figure 9 shows the inverted relaxation rate for the thicker layer, compare this with Figure 5.

Conclusions

The magnetization of a boundary layer increases rapidly with increasing magnetic Reynolds number based on the layer thickness λ_0. This thickness can be estimated as the time average of the integral of $v_z(0, t)$ from equation (80) during the ramp up of the linear beam, or $\lambda_0 = [v_z(0, t_\infty)t_\infty]/6$. This estimate produces $\lambda_0 = 2 \times 10^{-5}$ m for the conditions of the example of Figure 1. It seems likely that these hot, dense boundary layers with $\sigma\mu \approx 1$ expand with $R_M \approx 1$, and as a result are very highly magnetized. The examples show that electric and magnetic fields are all high below $x = 0.4$. Ions attempting to escape from the boundary layer by moving along the axial electric field must endure collisional drag, and overcome magnetic restraint. They are most likely to move as part of the thermal expansion of the magnetized plasma.

Auspices. This work was produced under the auspices of the U. S. DOE by LLNL under contract no. W-7405-Eng-48.

References

1. M. Garcia, "Self-effect in expanding electron beam plasma," Lawrence Livermore National Laboratory, UCRL-ID-134375, 7 May 1999, prepared for the 26th IEEE International Conference on Plasma Science, 2P22, 20-24 June 1999, Monterey, CA. http://www.llnl.gov/tid/lof/documents/pdf/235747.pdf

2. D. R. Welch, "Effects of electron-ion streaming due to beam-target interactions," Mission Research Corporation, presented at the DAHRT-2 Review, 16 January 1997.

3. P. W. Rambo and S. Brandon, "EM-PIC simulations of e-beam interaction with field emitted ions from bremsstrahlung targets," Lawrence Livermore National Laboratory, UCRL-JC-130469, 13 August 1998, prepared for the 19th International LINAC Conference, 23-28 August 1998, Chicago, IL.

4. W. M. Wood, B. L. Wright, D. M. Oró, R. D. Fulton, D. C. Moir, B. DeVolder, T. Kwan, "Dynamical measurements of plasmas generated by relativistic electrons colliding with metal targets," Los Alamos National Laboratory, prepared for the 25th IEEE International Conference on Plasma Science, 4C02, 1-4 June 1998, Raleigh, NC.

5. S. Sampayan, G. Caporaso, Y-J Chen, T. Houck, R. Richardson, J. Weir, G. Westenskow, C. Crist, M. Krogh, M. Garcia, "Experimental investigation of beam optics issues at the bremsstrahlung converters for radiographic applications," Lawrence Livermore National Laboratory, UCRL-JC-130417, 21 August 1998, prepared for the 19th International LINAC Conference, 23-28 August 1998, Chicago, IL.

6. T. Houck, S. Sampayan, M. Garcia, "Faraday cup measurements of the plasma plume produced at an x-ray converter," Lawrence Livermore National Laboratory, UCRL-JC-130422, 17 August 1998, prepared for the 19th International LINAC Conference, 23-28 August 1998, Chicago, IL.

7. G. J. Caporaso and Y-J Chen, "Analytic model of ion emission from the focus of an intense relativistic electron beam on a target," Lawrence Livermore National Laboratory, UCRL-JC-130594, 23 August 1998, prepared for the 19th International LINAC Conference, 23-28 August 1998, Chicago, IL.

8. T. J. T. Kwan and C. M. Snell, "Plasma and ion barrier for electron beam spot stability," Los Alamos National Laboratory, LA-UR-99-582, submitted to *Journal of Applied Physics*.

9. T. Houck and J. McCarrick, "The effect of trapped backstreaming ions on beam focus and emittance in radiographic accelerators," Lawrence Livermore National Laboratory, UCRL-JC-131946, March 1999, prepared for the Particle Accelerator Conference, 29 March-2 April 1999, New York, NY.

10. M. G. Haines, "Magnetic-field generation in laser fusion and hot-electron transport," *Canadian Journal of Physics*, Vol. 64, 1986, pages 912-919.

11. M. G. Haines, "Saturation mechanisms for the generated magnetic field in nonuniform laser-matter irradiation," *Physical Review Letters*, Vol. 78, No. 2, 13 January 1997, pages 254-257.

Figure captions

1. Magnetic induction for a linear beam. $B_\theta(x, t)$ in T for a linear beam with $I_0(0, t_\infty) = 6000$ A, $r_0 = 0.5$ mm, $j_\infty = 3.06 \times 10^{10}$ A/m, $t_\infty = 20$ ns, $B_\infty = 2.4$ T, and $kT_\infty/e = 37$ eV, which pierces a boundary layer of tantalum with $\lambda_0 = 2 \times 10^{-5}$ m and $\sigma = 10^6$ S/m. Five radial profiles are shown, at 4 ns, 8 ns, 12 ns, 16 ns, and 20 ns. Negative $B_\theta(x, t)$ values are plotted (positive numbers).

2. Radial electric field for a linear beam. $E_r(x, t)$ in V/m for Figure 1.

3. Axial electric field for a linear beam. $E_z(x, t)$ in V/m for Figure 1.

4. Axial velocity for a linear beam. $v_z(x, t)$ in m/s for Figure 1.

5. Radial profile of relaxation times. Inverted relaxation rate, in ns, for Figure 1.

6. Magnetic induction for thicker layer. $B_\theta(x, t)$ in T for a boundary layer with $\lambda_0 = 5 \times 10^{-5}$ m and all other parameters identical to those of the example of Figure 1. Negative $B_\theta(x, t)$ values are plotted (positive numbers).

7. Radial electric field for thicker layer. $E_r(x, t)$ in V/m for the thicker layer, compare this with Figure 2.

8. Axial electric field for thicker layer. $E_z(x, t)$ in V/m for the thicker layer, compare this with Figure 3.

9. Relaxation profile for thicker layer. $1/\omega(x)$ in ns for the thicker layer, compare this with Figure 5.

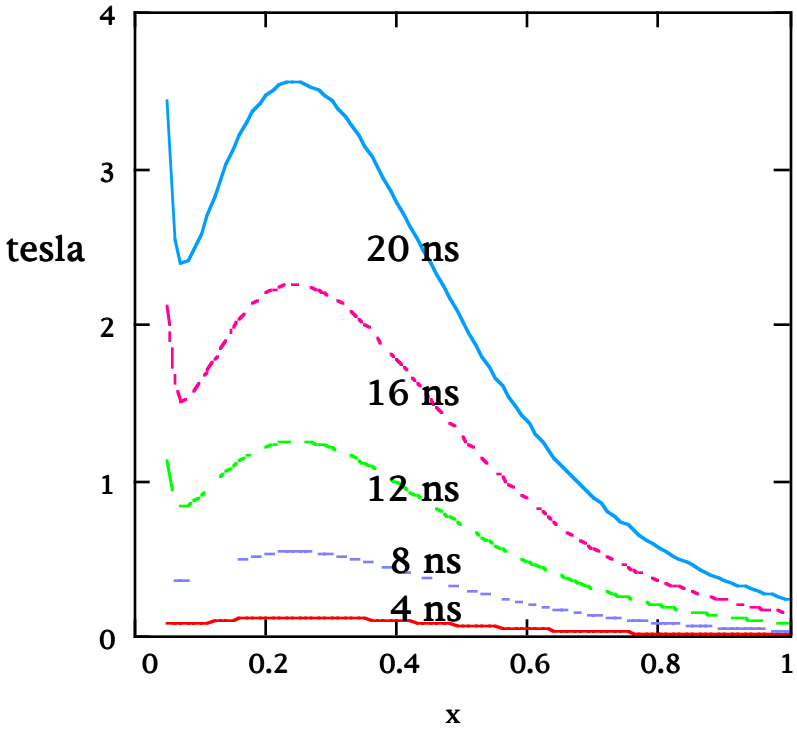

Figure 1, Magnetic induction for a linear beam

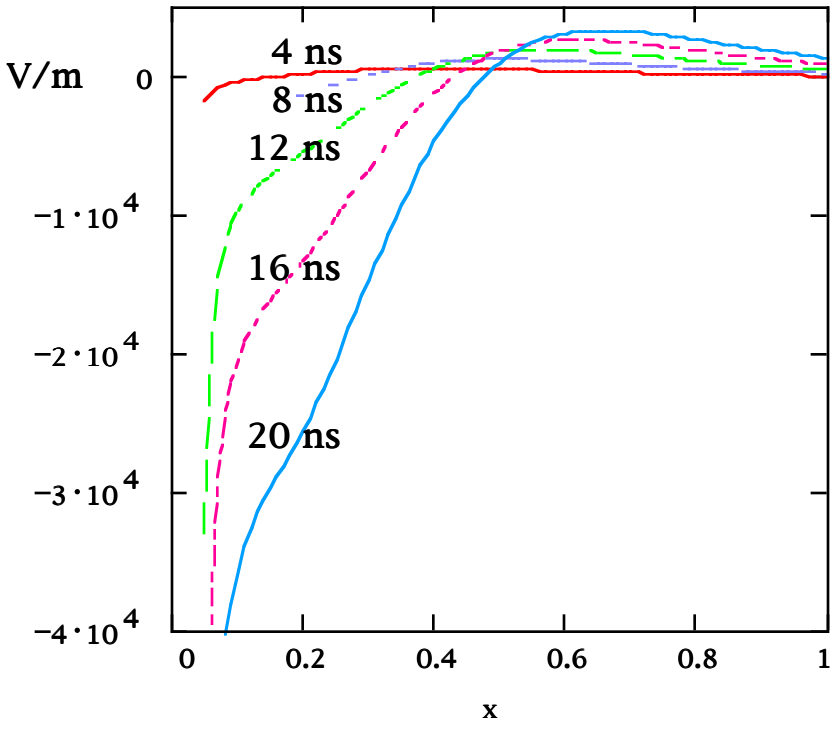

Figure 2, Radial electric field for a linear beam

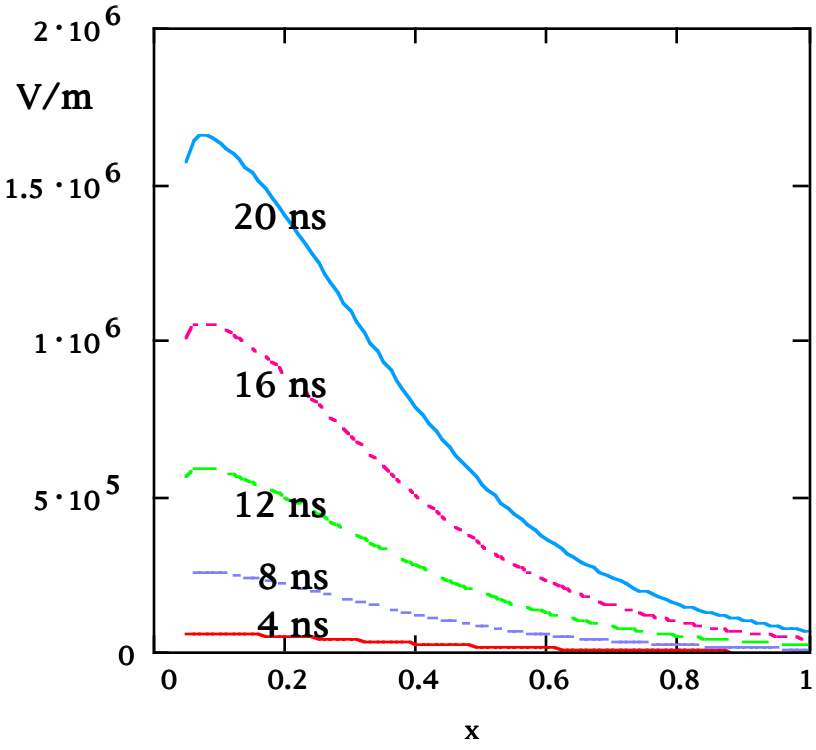

Figure 3, Axial electric field for a linear beam

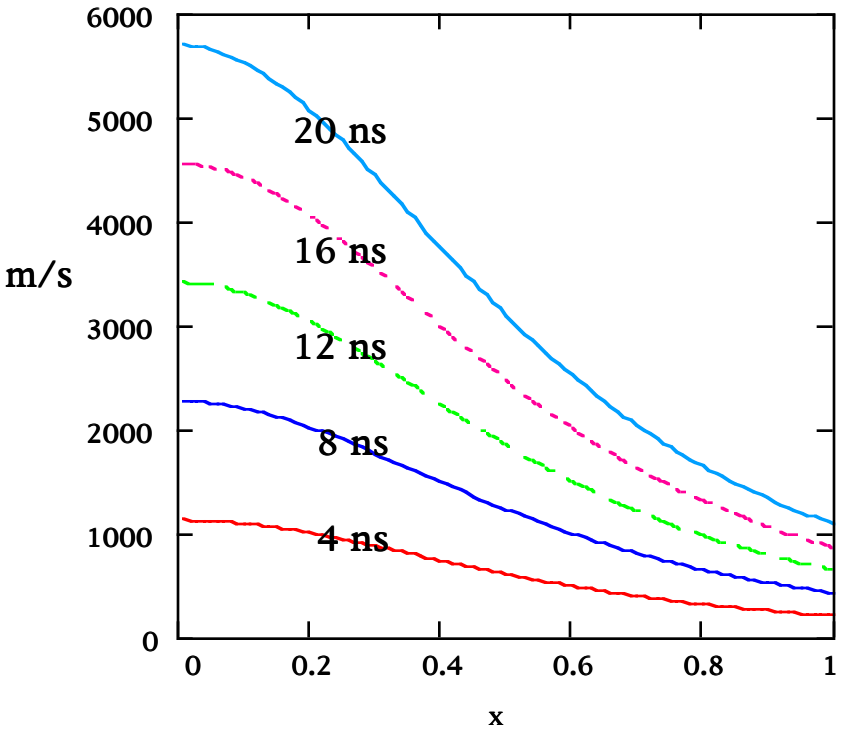

Figure 4, Axial velocity for a linear beam

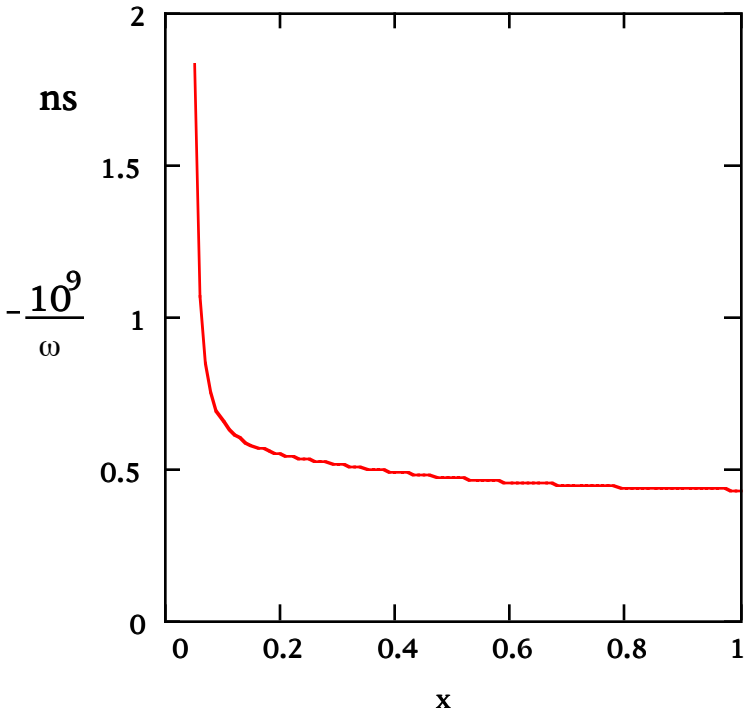

Figure 5, Radial profile of relaxation times

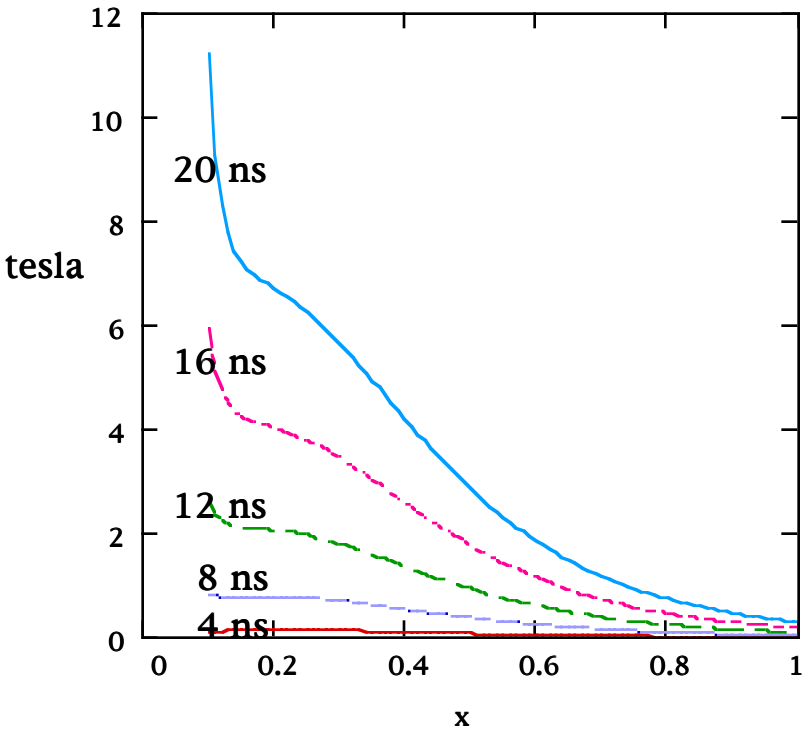

Figure 6, Magnetic induction for thicker layer

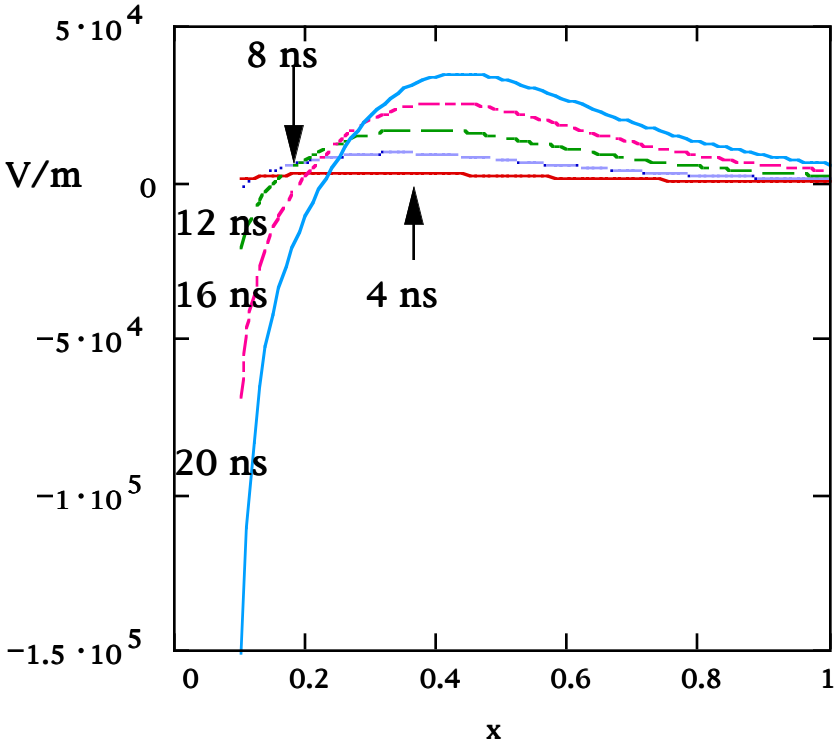

Figure 7, Radial electric field for thicker layer

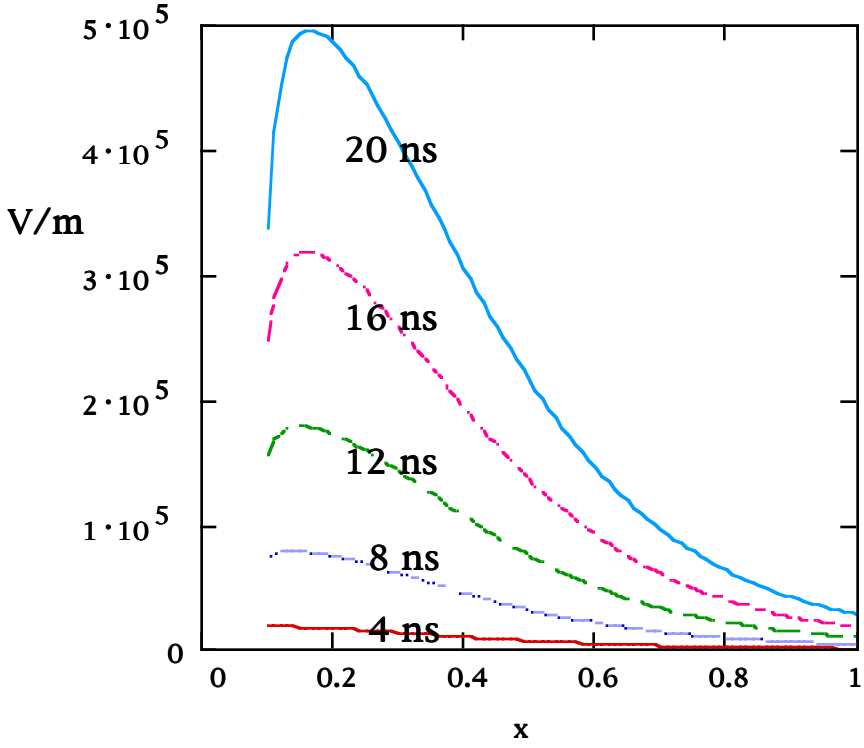

Figure 8, Axial electric field for thicker layer

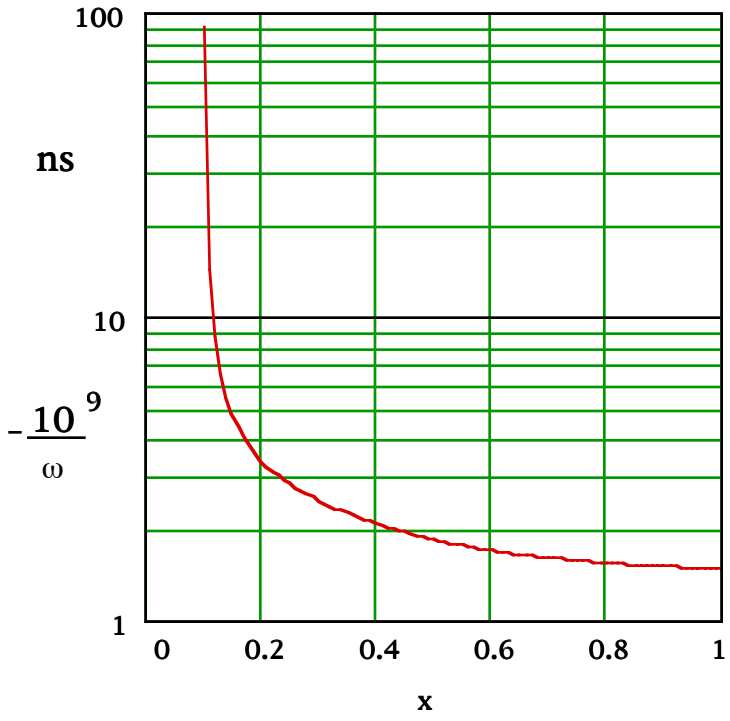

Figure 9, Relaxation profile for thicker layer